European Polymer Journal 197 (2023) 112365

Contents lists available at ScienceDirect

European Polymer Journal

journal homepage: www.elsevier.com/locate/europolj

Acidity/hydrogen peroxide-responsive PEGylated chitosan-modified polydopamine nanoparticles to realize effective photothermal conversion and intracellular drug delivery

Ming-Yen Shen, Yu-Hsin Chen, Nien-Tzu Yeh, Tzu-Hao Wang, Wen-Hsuan Chiang *

Department of Chemical Engineering, National Chung Hsing University, Taichung 402, Taiwan

ARTICLE INFO

Keywords:
Intracellular DOX delivery
Photothermal conversion
Polydopamine
PEGylated chitosan
pH-triggered drug release

ABSTRACT

To realize effective photothermal conversion and intracellular drug delivery for application of cancer treatment, an acidity/hydrogen peroxide-responsive nanoparticle system comprising melanin-like polydopamine (PDA) as the hydrophobic core covered by PEGylated chitosan (PEG-CS) conjugates is created herein. The PEG-CS/PDA nanoparticles characterized with a well-dispersed spherical shape exhibited prominent colloidal stability in the milieu of physiological salt concentration. Through π- π stacking and hydrophobic interactions between doxorubicin (DOX) and PDA, DOX molecules were efficiently incorporated into the PEG-CS/PDA nanoparticles. With solution pH being adjusted from 7.4 to 5.0, the ionic complexation of protonated chitosan with negatively-charged PDA enabled the embedding of outer PEG segments of DOX@PEG-CS/PDA nanoparticles into the neutral and gel-like surfaces, thus eliciting interparticle aggregation. The same pH stimulation also accelerated DOX release due to the declined interactions of DOX and PDA combined with enhanced repulsion force between positively-charged chitosan and DOX. Notably, the PEG-CS/PDA nanoparticles not only showed robust photothermal effect and stability, but also were significantly degraded by hydrogen peroxide. After being endocytosed by TRAMP-C1 cells, the DOX@PEG-CS/PDA nanoparticles gradually released drug within acidic organelles, thus promoting drug accumulation in nuclei to kill cancer cells. This work indicates the feasibility for applying such DOX@PEG-CS/PDA nanoparticles in cancer treatment.

1. Introduction

In the past decades, the incidence of cancer has constantly raised, posing a significant threat to human life. Despite the availability of various clinical strategies in antitumor therapeutics, including chemotherapy, surgery and radiotherapy, cancer continues to be one of the most fatal diseases worldwide [1,2]. Due to their convenience, low cost and high availability, chemotherapy drugs are among the most commonly used anticancer reagents [1]. Conventional cancer chemotherapy is mostly executed by small-molecule compounds, unfortunately, these small-molecule drugs are non-specifically distributed in healthy organs and tissues due to lack of tumor targeting, thereby causing serious adverse effects [1,3,4]. To address these issues, it is vital to create functionalized drug delivery systems (DDSs) capable of minimizing systemic non-specific exposure and selectively liberating drugs at tumor sites. In recent years, versatile organic and inorganic nanoparticles, including liposomes [5,6], polymeric micelles and assemblies [7–10], nanoceramics [10–13] and metal–organic frameworks (MOF) [14,15] have been extensively developed as DDSs because of their ability to passively target tumor upon the enhanced permeability and retention (EPR) effect and control drug release in response to external stimulus, thus declining the side effects of chemotherapy. Among these DDSs, the melanin-like polydopamine (PDA) nanoparticles have attracted considerable attention owing to their good biocompatibility and biodegradation, satisfied photothermal conversion efficiency and effective combination with small-molecule drugs or tumor-targeting ligands on the surface by diverse interactions [9,16–22]. However, the pristine PDA nanoparticles have tendency of adhering various biomolecules such as protein and cells [23,24] and aggregating in salt-containing physiological solutions [16,18]. Such a poor colloidal stability of PDA nanoparticles in the physiological environment largely limited their clinical application in tumor-targeted drug delivery.

In order to improve feasibility of PDA nanoparticles utilized as DDS for cancer therapy, it is urgent to boost their colloidal stability by proper

* Corresponding author.
E-mail address: whchiang@dragon.nchu.edu.tw (W.-H. Chiang).

https://doi.org/10.1016/j.eurpolymj.2023.112365
Received 20 May 2023; Received in revised form 5 August 2023; Accepted 11 August 2023
Available online 12 August 2023

surface modification. In this end, through Michael addition or Schiff base reaction, a varied of thiol- or amine-containing macromolecules such as poly(ethylene glycol) (PEG) [25–27], polysaccharides [16,28–30] and phosphorylcholine-based polymers [31] were covalently conjugated with the catechol/quinone groups on the surfaces of PDA nanoparticles. Because these polymers bind strongly with water molecules via hydrogen bonding, a thin hydration layer can be formed, thus preventing the aggregation of PDA nanoparticles and non-specific adsorption of proteins [32]. Among these polymers, PEG has been extensively used to decorate the surfaces of PDA nanoparticles due to its excellent hydrophilicity, biocompatibility and flexibility [33,34]. For example, Liu's group reported that PDA nanoparticles after modification with amine-terminated PEG exhibited outstanding stability in various physiological solutions and successfully carried several different radionuclides such as ^{99m}Tc and ^{131}I, as well as a chemotherapy drug doxorubicin (DOX), thus realizing nuclear-imaging-guided combined radioisotope therapy and chemotherapy of cancer in one system [35]. In similar way, the mesoporous PDA nanoparticles modified with PEG-NH_2 were utilized as vehicles of indocyanine green (ICG) and dimethylcurcumin (DMC) for combination therapy of castration-resistant prostate cancer [26]. In addition to PEG, in the past few years, various polysaccharides including hyaluronic acid [28], alginate [30] and hydroxyethyl starch (HES) [16] have been adopted to decorate PDA nanoparticles due to their good biocompatibility and biodegradability. For instance, as presented in the study of Li and coworkers [16], the thiol-modified HES can be covalently attached to the surface of PDA nanoparticles. The attained HES-PDA nanoparticles employed as DOX carriers not only exhibited good stability, high drug loading efficiency, favorable lyophilization stability and biocompatibility, but also effectively inhibited liver tumor growth without significant side effect associated with DOX.

Distinct from the aforementioned studies on the surface modification of PDA nanoparticles with either linear PEG or polysaccharides alone, in this work, the graft-type PEGylated chitosan (PEG-CS) conjugates were synthesized and chemically decorated on the surfaces of PDA nanoparticles upon Michael addition or Schiff base reaction between PEG-CS conjugates and PDA nanoparticles. To the best of our knowledge, few studies on the surface decoration of PDA nanoparticles with PEG-grafted polysaccharide has been reported [18]. The obtained PEG-CS/PDA nanoparticles showed prominent colloidal stability in aqueous solutions of physiological salt concentration and were utilized as DOX vehicles. Furthermore, the effects of weight ratio of PEG-CS conjugates to PDA nanoparticles in feed on the colloidal stability of PEG-CS/PDA nanoparticles were further investigated. The structural characteristics of PEG-CS/PDA nanoparticles with or without DOX loading were explored by angle-dependent dynamic/static light scattering (DLS/SLS), transmission electron microscopy (TEM), scanning electron microscopy (SEM) and zeta potential measurements. Also, in addition to the in vitro DOX release performance and hydrogen peroxide-triggered degradation, the photothermal conversion effect of PEG-CS/PDA nanoparticles was evaluated. The in vitro cellular uptake of DOX@PEG-CS/PDA nanoparticles by TRAMP-C1 cells and their anticancer potency were further assessed.

2. Experimental section

2.1. Materials

DOX (in the hydrochloride salt form) was purchased from Carbosynth Ltd. (UK). Chitosan oligosaccharide (MW 5.0 kDa, 81 % degree of deacetylation) was obtained from Glentham Life Science Ltd. (UK). Methoxy poly(ethylene glycol) (mPEG) (MW 5.0 kDa), 3-(4,5-Dimethylthiazol-2-yl)-2,5-diphenyltetrazolium bromide (MTT) and D_2O (99.9 atom % D) were purchased from Sigma-Aldrich (USA). N-(3-Dimethylaminopropyl)-N'-ethylcarbodiimide hydrochloride (EDC, 95 %) was attained from Matrix Scientific (USA). Dopamine hydrochloride (DA), N-hydroxysuccinimide (NHS, 98%) and succinic anhydride (99%) were acquired from Alfa Aesar (USA). Fetal bovine serum (FBS) was purchased from Hyclone (USA). Hoechst 33,342 was purchased from Invitrogen. Deionized water was produced from Milli-Q Synthesis (18 MΩ, Millipore). All other chemicals were reagent grade and used as received. TRAMP-C1 cells (murine prostate cancer cell line) were acquired from Food Industry Research and Development Institute (Hsinchu City, Taiwan).

2.2. Synthesis and characterization of PEG-CS conjugates

According to our previous work [36], the mPEG-COOH employed in this study was attained upon the ring-opening reaction of succinic anhydride with mPEG. The PEG-CS conjugates were synthesized by the EDC/NHS-mediated amidation of chitosan and mPEG-COOH (Scheme 2). In brief, EDC (227 mg) was added into deionized water (4.0 mL) containing chitosan (100 mg), mPEG-COOH (295 mg) and NHS (136 mg). The reaction was carried out under stirring at 25 °C for 48 h, followed by dialysis (Cellu Sep MWCO 6000 ~ 8000) with deionized water to remove NHS and EDC. The product was then collected by lyophilization. The PEG-CS conjugates were characterized by Fourier transform infrared (FT-IR) (FT-720 spectroscopy, HORIBA, Japan) using KBr pellet for the sample preparation. The degree of substitution (DS) of chitosan with mPEG-COOH defined as the number of mPEG segments per 100 glucosamine units was determined by proton nuclear magnetic resonance (^{1}H NMR) (Agilent DD2 600 MHz NMR spectrometer) using D_2O as the solvent at 25 °C.

2.3. Preparation of PEG-CS/PDA nanoparticles

PDA nanoparticles were first synthesized by the oxidative self-polymerization of DA under alkaline conditions. In brief, DA (37.5 mg) dissolved in deionized water (20 mL) was mixed with 1 N NaOH solution (150 μL). The reaction was performed under mild stirring at 50 °C for 5 h, followed by dialysis (Cellu Sep MWCO 12000 ~ 14000) against pH 8.5 phosphate buffer at 4 °C to remove unreacted DA molecules. The PEG-CS/PDA nanoparticles were prepared as follow. The purified PDA nanoparticle solution (0.9 mL, 1.1 mg/mL) was dropwise added into 0.1 mL of pH 7.0 Tris buffer containing PEG-CS conjugates (0.1, 0.2, 0.4, 0.8 and 1.2 folds with respect to weight of PDA nanoparticles in feed) and then stirred at room temperature for 24 h, followed by dialysis (Cellu Sep MWCO 12000 ~ 14000) against pH 8.5 Tris buffer at 4 °C for 24 h.

2.4. Preparation of DOX@PEG-CS/PDA nanoparticles

The DOX@PEG-CS/PDA nanoparticles were prepared as follow. 0.85 mL of PDA nanoparticle solution (1.2 mg/mL) was dropwise added into 0.1 mL of pH 7.0 5.0 mM Tris buffer containing PEG-CS conjugates (1.2 mg) and then stirred at room temperature for 1 h, followed by the addition of DOX solution (50 μL, 2 mg/mL). The resulting solution was then stirred in dark at room temperature for 12 h and dialyzed (Cellu Sep MWCO 12000 ~ 14000) against pH 8.5 Tris buffer at 4 °C for overnight to remove unloaded DOX molecules.

2.5. Structural characterization

The absorption spectra of PEG-CS/PDA and DOX@PEG-CS/PDA nanoparticles in pH 7.4 phosphate buffer were acquired by a UV/Vis spectrophotometer (U-2900, Hitachi, Japan). X-ray photoelectron spectroscopy (XPS) analysis was performed by a PHI 5000 VersaProbe III X-ray photoelectron spectrometer (ULVAC-PHI, Japan) with AlKα radiation ($h\gamma = 1486.6$ eV) at 15 kV and 150 W. Thermogravimetric analysis (TGA) was performed with thermogravimetric analyzer EXSTAR TG/DTA 6200 (Seiko Instruments Inc) in a N_2 atmosphere by heating the sample to 900 °C at the rate of 10 °C/min. The mean hydrodynamic

diameter, particle size distribution (polydispersity index, PDI), root-mean-square radius of gyration (R_g) and angle-dependent autocorrelation functions of various PDA-containing nanoparticles in aqueous solutions were obtained by DLS/SLS measurements with Brookhaven BI-200SM goniometer equipped with a BI-9000 AT digital correlator using a solid-state laser (35 mW, $\lambda = 637$ nm). For the above nanoparticles, their R_g value was quantitatively determined using the Berry plot of the scattering intensity ($I_{ex}^{1/2}$) versus the square of the scattering vector (q^2) from the angle-dependent measurements of the light scattering intensity. The zeta potential of various nanoparticles in aqueous solutions of different pH was measured by a Litesizer 500 (Anton Paar, USA). The data about particle size and zeta potential presented herein represent an average of at least triplicate measurements. The morphology of various PDA-based nanoparticles was examined by TEM (HT7700, Hitachi, Japan) and SEM (JEOL JSM-7800F Prime Schottky Field Emission SEM, Japan).

2.6. DOX loading efficiency and content

To quantify the amount of DOX loaded within PEG-CS/PDA nanoparticles, a prescribed volume (10 μL) of the DOX@PEG-CS/PDA nanoparticle solutions was lyophilized and suspended in 1.0 mL of DMSO to isolate drug from nanoparticles. After the solution was sonicated for 15 min and centrifuged at 10000 rpm for 2 min, the supernatant was taken out for analysis of drug concentration. The DOX fluorescence in the range 500–700 nm was measured by a Hitachi F-2700 fluorescence spectrometer. The calibration curve utilized for drug loading characterization was established by fluorescence intensity of DOX with various concentrations in DMSO (Fig. S1). The drug loading efficiency (DLE) and drug loading content (DLC) were calculated as follow:

DLE (%) = (weight of loaded DOX/weight of DOX in feed) × 100%.

DLC (%) = (weight of loaded DOX/total weight of the DOX@PEG-CS/PDA nanoparticles) × 100%.

2.7. In vitro DOX release performance

For in vitro DOX release measurement, the DOX@PEG-CS/PDA nanoparticle solution (1.0 mL) was dialyzed (Cellu Sep MWCO 12000 ~ 14000) against pH 7.4 phosphate buffer saline (PBS) and pH 5.0 acetate buffer (20 mL), respectively, at 37 °C under gentle shaking (100 rpm). The 1.0 mL of dialysate was taken out periodically for analysis and replaced with an equal volume of fresh buffer. The amount of DOX liberated was determined by fluorescence measurements as described above.

2.8. Near-infrared (NIR)-triggered photothermal conversion

Various PDA-based nanoparticles were dispersed in aqueous solutions of pH 7.4 and 5.0 (1.0 mL), and then irradiated with a NIR laser of 808 nm (1.0 W/cm^2) for 5 min. The solution temperatures were recorded with an infrared thermal imaging camera (Thermo Shot F20, NEC Avio Infrared Technologies, Germany). To assess the photostability, the PEG-CS/PDA nanoparticle solution (PDA concentration: 200 μg/mL) was exposed to irradiation of 808 nm NIR laser (1.0 W/cm^2) for 5 min and then cooled down to ambient temperature by turning off the light source. During three on/off cycles, the temperature change of PEG-CS/PDA nanoparticle solution was monitored by above instrument. According to the data from the first cooling status, the photothermal conversion efficiency of PEG-CS/PDA nanoparticles was calculated by the previously reported method [18].

2.9. In vitro cellular uptake

TRAMP-C1 cells (2×10^5 cells/well) seeded onto 22 mm round glass coverslips in 6-well plates were separately incubated with free DOX molecules and DOX@PEG-CS/PDA nanoparticles (DOX concentration = 10 μM) at 37 °C for 1 and 4 h. After two washes with HBSS and immobilization with 4 % formaldehyde, the cell nucleus was stained with Hoechst 33,342 for 15 min. The cellular images were obtained using a confocal laser scanning microscope (CLSM) (Olympus, FluoView FV3000, Japan) equipped with a Hoechst set (Ex. 405 nm) and a DOX set (Ex. 488 nm).

2.10. In vitro cytotoxicity examination

In this study, cell viability was determined by MTT assay. First, TRAMP-C1 cells (1×10^4 cells/well) were seeded in a 96-well plate and incubated with DMEM containing 10% FBS and 1% penicillin at 37 °C for 24 h. The spent medium was then replaced with 100 μL of fresh medium containing free DOX molecules or DOX@PEG-CS/PDA nanoparticles at varying DOX concentrations or DOX-free nanoparticles, and the cells were further incubated for 24 h. Subsequently, the MTT solution (100 μL, 0.25 mg/mL) was added into each well, followed by incubation at 37 °C for 3 h. After discarding the culture medium, DMSO (120 μL) was added into each well to dissolve the precipitate, and the absorbance at 570 nm was measured using a BioTek 800TS microplate reader.

2.11. Statistical analysis

Data are reported as mean ± SD. The differences among groups were determined using one-way or two-way ANOVA analysis; ns > 0.05, *$p < 0.05$, **$p < 0.01$, ***$p < 0.001$.

3. Results and discussion

3.1. Synthesis and characterization of PEG-CS conjugates

Through the NHS/EDC-mediated amide bond formation between chitosan oligosaccharide and mPEG-COOH, the PEG-CS conjugates used in this work were synthesized and characterized by FT-IR and ^{1}H NMR measurements. As revealed in the FT-IR spectrum of PEG-CS conjugates (Fig. S2), in addition to the feature absorption bands of C-O and C–C stretching vibration of mPEG-COOH at 1112 and 955/841 cm^{-1}, respectively, the absorption bands at 3450 cm^{-1} for NH_2 and OH stretching vibration, and at 1662, 1562 and 1467 cm^{-1} for C = O stretching vibration, N–H bending vibration and C-N stretching vibration of amide groups, respectively, from chitosan were observed. The ^{1}H NMR spectrum of PEG-CS conjugates showed the appearance of the characteristic proton signals of mPEG at δ 3.7 and 3.4 ppm, respectively, and of chitosan at δ 3.5–4.0 2.8 and 2.1 ppm, respectively (Fig. 1). These results confirm the successful conjugation of chitosan with mPEG-COOH. Based on the integral ratio of the signals of the methoxy protons from mPEG-COOH at δ 3.4 ppm to the acetyl protons from chitosan at δ 2.1 ppm, the DS of chitosan with mPEG-COOH was calculated to be ca 8.8.

3.2. Preparation and characterization of PDA and PEG-CS/PDA nanoparticles

As presented in Scheme 1a, PDA nanoparticles were attained by self-polymerization of DA molecules in NaOH solution at 50 °C. The UV/Vis spectra showed that DA monomers in aqueous solution exhibited a narrow absorption peak at 281 nm, while PDA nanoparticles displayed remarkably increased absorption from visible light to NIR light (Fig. 2a). In the FT-IR spectrum of PDA nanoparticles (Fig. S2), in addition to feature absorption bands of OH stretching vibration at 3450 cm^{-1}, two weak typical absorption bands of indole and indoline structure at 1607 and 1508 cm^{-1}, respectively, were observed. These findings signify the successful oxidative self-polymerization of DA molecules into PDA nanoparticles. The attained PDA nanoparticles dispersed in pH 7.4 0.01

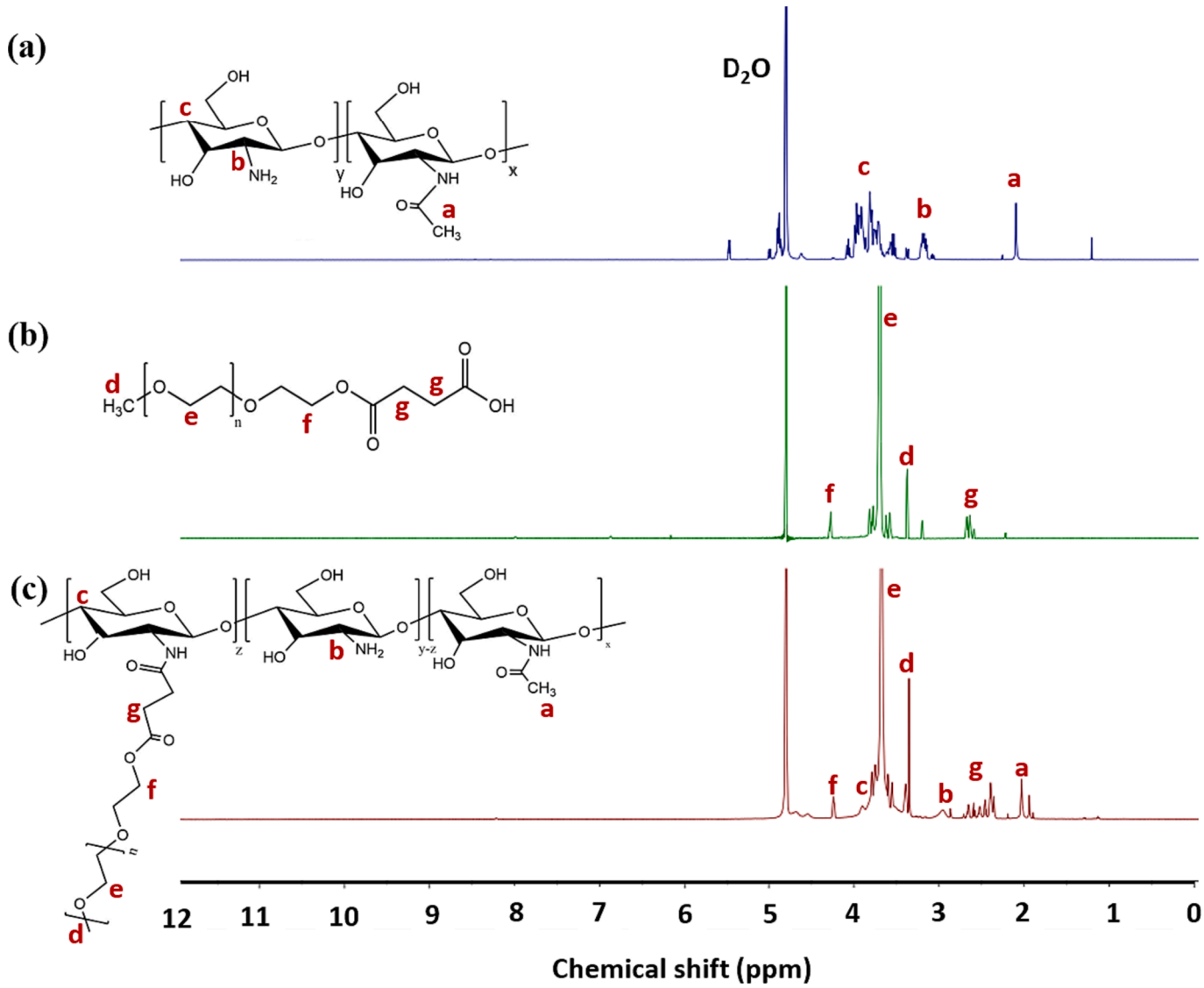

Fig. 1. ^{1}H NMR spectra of (a) chitosan, (b) mPEG-COOH and (c) PEG-CS.

M phosphate buffer exhibited mean hydrodynamic diameter (D_h) of ca 118.8 ± 5.7 nm and mono-modal size distribution (PDI ca 0.15) (Table 1 and Fig. 2b). Notably, when the PDA nanoparticles were dispersed in pH 7.4 0.15 M PBS for 1 h, particle aggregation occurred as evidenced by the significantly enlarged particle size over 600 nm. Such a severe aggregation of bare PDA nanoparticles at the salt concentration higher than 10 mM could be ascribed to that their surface charges have been largely shielded by salt ions as reported elsewhere [16,18,27].

To improve colloidal stability of PDA-based nanoparticles under physiological environment for their better applications of cancer nanomedicine, the surfaces of PDA nanoparticles were covalently modified with the hydrophilic PEG-CS conjugates. Compared to the N1s XPS spectrum of PDA nanoparticles (Fig. 2c), the feature peaks of pyridinc N (397.8 eV) and pyrrolic N (401.4 eV) from PDA segments, and the peaks of amine (398.5 eV) and amide (400.5 eV) from PEG-CS conjugates were observed in the N1s XPS spectrum of PEG-CS/PDA nanoparticles (Fig. 2d). Furthermore, different from PDA nanoparticles with quite high intensity of C = C peak, the PEG-CS/PDA nanoparticles showed the lower intensity of feature peak of C = C (284.1 eV) relative to that of C–C, C-N and C-O as revealed in Fig. S3. Note that the content of nitrogen atom of PDA nanoparticles after being modified with PEG-CS conjugates was appreciably reduced from 9.3 to 3.2 % as revealed in XPS data (Table 2 and Fig. S4). The findings clearly indicate the successful incorporation of PEG-CS coating layer with PDA cores. As shown in Fig. S5, when the weight ratio of PEG-CS and PDA in feed was adjusted from 0 to 1.2, the particle size of PEG-CS/PDA nanoparticles dispersed in pH 7.4 0.01 M phosphate buffer was somewhat increased from 118.8 to 149.7 nm. The enlarged particle size could be attributed to the presence of additional PEG-CS-constituted layer covering the PDA cores. Notably, the PDA nanoparticles after being decorated with PEG-CS conjugates (PEG-CS/PDA weight ratio = 1.2) exhibited the appreciable conversion in zeta potential from −30.2 to −14.8 mV (Fig. 2e), suggesting that the PEG-CS surface coating could largely shield the negatively-charged phenolic hydroxyl groups of PDA cores. When the PEG-CS/PDA weight ratio in feed was raised from 0.1 to 1.2, the attained PEG-CS/PDA nanoparticles in pH 7.4 0.15 M PBS or 0.01 M phosphate buffer showed virtually similar particle size (Fig. 2f and S5). This strongly demonstrates that the adequate number of PEG-CS conjugates attached on the surfaces of PDA cores could effectively avoid the salt-induced inter-particle aggregation, thus endowing the hybrid nanoparticles with robust colloidal stability by PEG-mediated steric repulsion effect. Therefore, the PEG-CS/PDA nanoparticles fabricated from the coupling of PEG-CS and PDA at a weight ratio of 1.2 were selected as DOX vehicles due to their sound colloidal stability.

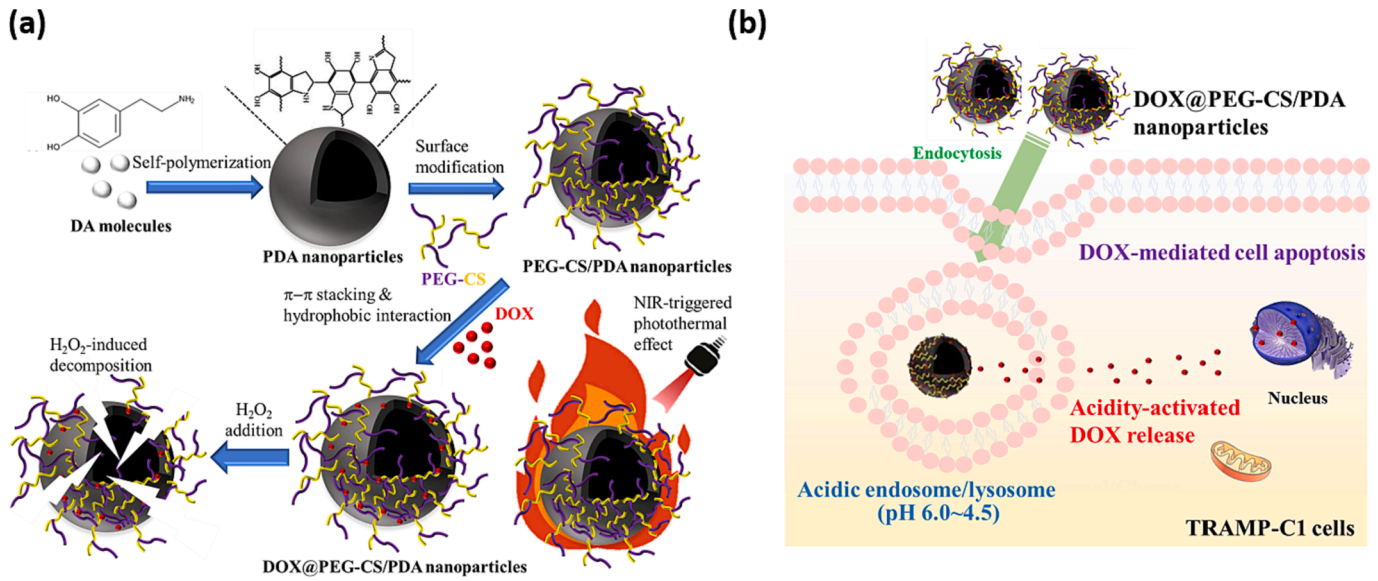

Scheme 1. Illustration of (a) preparation of DOX@PEG-CS/PDA nanoparticles and their NIR-triggered hyperthermia and H_2O_2-induced decomposition, and (b) intracellular drug delivery of DOX@PEG-CS/PDA nanoparticles to elicit apoptosis of cancer cells.

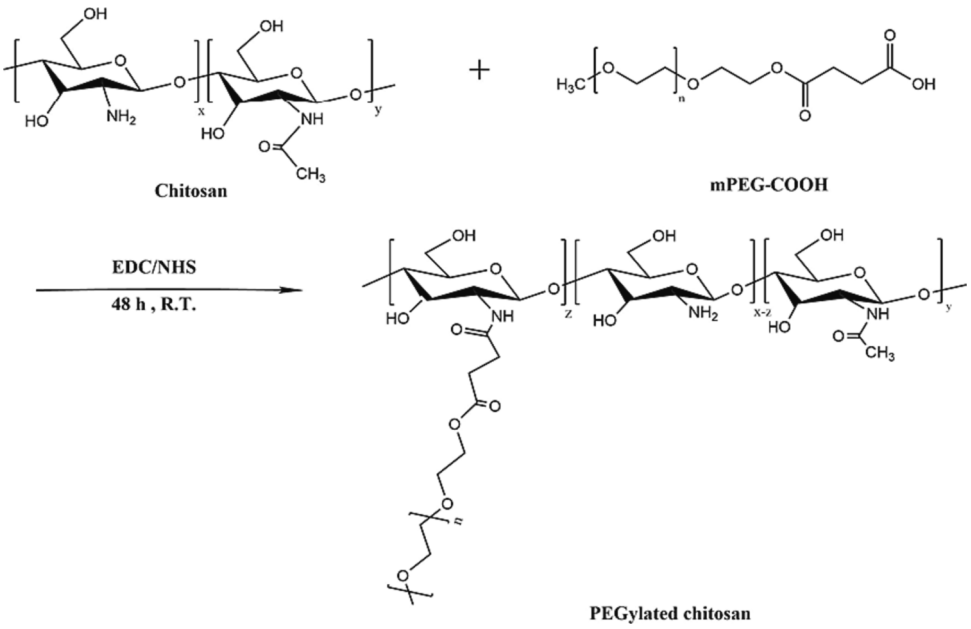

Scheme 2. Synthetic route and chemical structure of PEG-CS conjugates.

As shown in TGA profiles (Fig. 3a), the PEG-CS/PDA nanoparticles (PEG-CS/PDA weight ratio = 1.2) consist of ca 49.2 wt% PEG-CS and 52.8 wt% PDA. The result illustrates that ca 77.7 % of the added PEG-CS conjugates could be chemically coupled on the surfaces of PDA cores. Next, the morphology of PEG-CS/PDA nanoparticles was explored by the angle-dependent DLS/SLS and TEM examination. A high linear relationship between the relaxation frequency (Γ) and q^2 was attained in the DLS data of PEG-CS/PDA nanoparticles in pH 7.4 PBS (Fig. 3b), signifying that the hybrid nanoparticles displayed a spherical shape [37,38]. Furthermore, the R_g of PEG-CS/PDA nanoparticles in pH 7.4 PBS was determined by SLS to be ca 62.3 nm (Fig. 3b) and the ratio of R_g to hydrodynamic radius (R_h) was thus obtained to be 0.81, being comparable to that (0.77) of uniform solid sphere-like particles [37,39,40]. Also, the TEM images of bare PDA nanoparticles and PEG-CS/PDA nanoparticles further illustrated their well-dispersed solid-like spherical form (Fig. 3c). It is worth mentioning that the particle size (ca 120.5 nm) of PEG-CS/PDA nanoparticles is similar to that of PDA nanoparticles observed by TEM, but is appreciably smaller than that (ca 149.7 nm) of the counterparts measured by DLS. This can be ascribed to the structural transition of the PEG-CS coating layers of hybrid nanoparticles from hydrated (DLS) to dry (TEM) state, leading to non-swelling of coating layer. Based on the angle-dependent DLS/SLS data and TEM images, the hybrid PEG-CS/PDA nanoparticles were further demonstrated to have a spherical shape comprising a hydrophobic PDA core covered by hydrated PEG-CS layers (Scheme 1).

Due to the inherent pH-responsive property of chitosan segments from PEG-CS conjugates, the PEG-CS/PDA nanoparticles were expected to show the structural transformation in response to external pH change. When the solution pH was adjusted from 7.4 to 5.0, different from no significant variation in particle size of bare PDA nanoparticles (Fig. 3d),

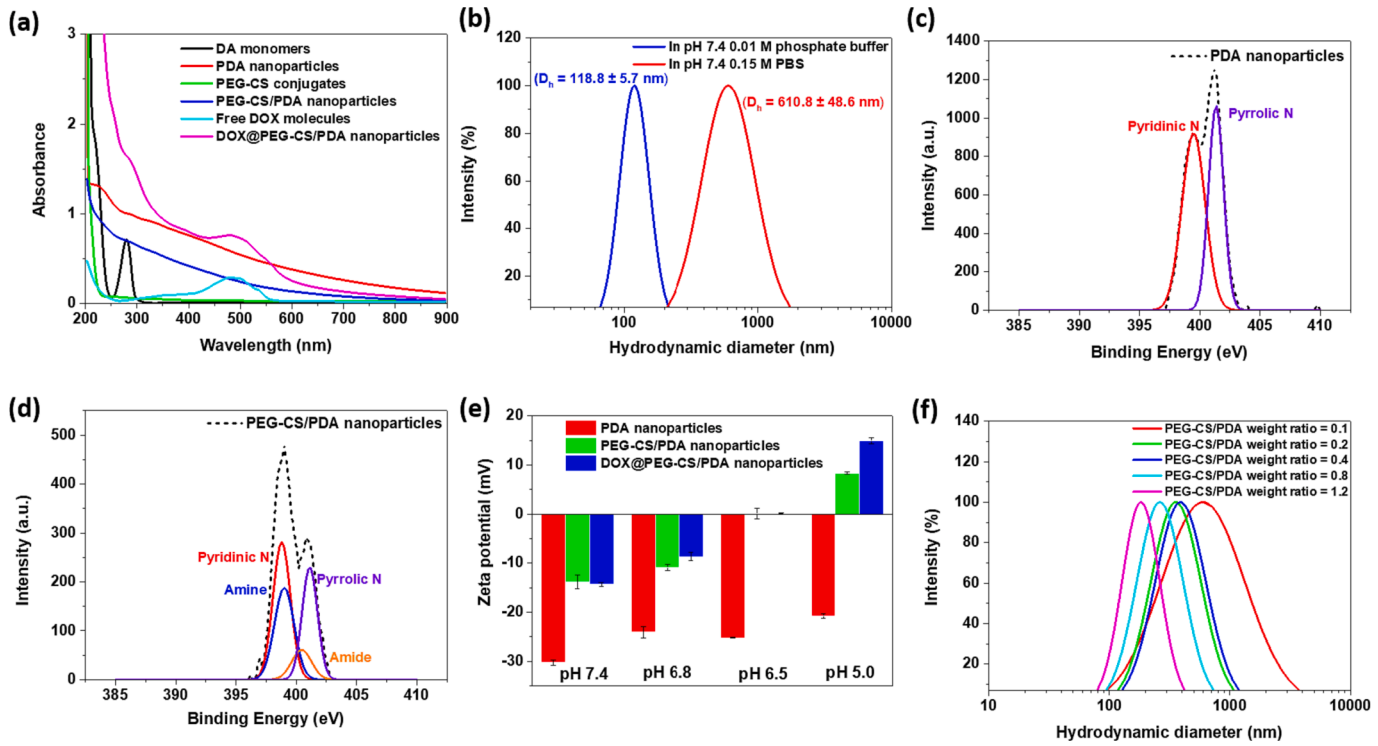

Fig. 2. (a) UV/Vis spectra of DA monomers, PDA nanoparticles, PEG-CS conjugates, PEG-CS/PDA nanoparticles, free DOX molecules and DOX@PEG-CS/PDA nanoparticles in aqueous solutions. (b) DLS particle size distribution profiles of pristine PDA nanoparticles separately dispersed in pH 7.4 0.01 M phosphate buffer and 0.15 M PBS for 1 h. N1s XPS spectra of (c) PDA nanoparticles and (d) PEG-CS/PDA nanoparticles. (e) Zeta potential values of various nanoparticles in aqueous solutions of different pH. (f) DLS particle size distribution profiles of PEG-CS/PDA nanoparticles with different PEG-CS/PDA weight ratios in pH 7.4 0.15 M PBS.

Table 1
DLS characteristics and drug loading capacities of various PDA-based nanoparticles.

Sample	D_h (nm)	PDI	DLE (%)	DLC (wt %)
PDA nanoparticles	118.8 ± 5.7	0.15 ± 0.08	–	–
PEG-CS/PDA nanoparticles	149.7 ± 2.3	0.21 ± 0.01	–	–
DOX@PEG-CS/PDA nanoparticles	174.4 ± 1.2	0.20 ± 0.02	69.9 ± 1.9	4.8 ± 0.7

Table 2
Different atomic content of PEG-CS conjugates, PDA nanoparticles and PEG-CS/PDA nanoparticles determined by XPS.

Sample	C atomics (%)	O atomics (%)	N atomics (%)
PEG-CS conjugates	67.9	30.4	1.8
PDA nanoparticles	58.8	31.9	9.3
PEG-CS/PDA nanoparticles	63.6	33.2	3.2

the particle size of PEG-CS/PDA nanoparticles was remarkably increased from 149.7 to beyond 2000 nm (Fig. 3e). In agreement with DLS data, massive inter-particle aggregation of PEG-CS/PDA nanoparticles at pH 5.0 was observed by TEM (Fig. 3c). Notably, with solution pH being reduced from 7.4 to 6.5 and 5.0, compared to slight variation in the zeta potential of PDA nanoparticles, the zeta potential of PEG-CS/PDA nanoparticles was converted from −14.8 to around 0 mV and + 8.4 mV (Fig. 2e). Obviously, the PEG-CS/PDA nanoparticles exhibited virtually neutral or somewhat positively-charged surfaces in response to the pH reduction owing to the increased protonation of primary amine groups within PEG-CS layers, while the PDA nanoparticles still maintained negatively-charged surfaces under the same pH stimulation due to the exposure of phenolic hydroxyl groups. Based on the above findings, such a considerable aggregation of PEG-CS/PDA nanoparticles in weak acidic milieu could be attributed to that the positively-charged chitosan segments of PEG-CS layers have high tendency of forming electrostatic complexes with negatively-charged phenol groups of PDA cores, thereby facilitating embedding of outer PEG segments of hybrid nanoparticles into nearly neutral surfaces to elicit particle aggregation in the absence of electrostatic repulsion force and steric stabilization (Fig. 3f). By contrast, due to the lack of pH-responsive coating layer, the PDA nanoparticles retained stable colloidal dispersion by negatively-charged surfaces in response to external pH change from 7.4 to 5.0. Notably, once the PEG-CS/PDA nanoparticles were dispersed in aqueous solutions of physiological salt concentration (0.15 M), the pH-induced inter-particle aggregation effect was further enhanced as presented in Fig. S6.

3.3. Preparation and characterization of DOX@PEG-CS/PDA nanoparticles

By the π - π stacking and hydrophobic interaction of DOX molecules and aromatic ring-rich PDA cores, DOX molecules were incorporated into hybrid nanoparticles to obtain DOX@PEG-CS/PDA nanoparticles. Distinct from PEG-CS/PDA nanoparticles, DOX@PEG-CS/PDA nanoparticles exhibited the characteristic absorption peak of DOX at 480 nm in the UV/Vis spectrum (Fig. 2a). The DLE and DLC of DOX@PEG-CS/PDA nanoparticles were determined to be ca 69.9 % and 4.8 wt%, respectively (Table 1). Notably, at the same drug concentration, DOX fluorescence intensity of DOX@PEG-CS/PDA nanoparticles was appreciably lower compared to that of free DOX molecules (Fig. 4a), being ascribed to the strong fluorescence quenching ability of PDA core [41]. These results illustrate the robust attachment of DOX on hybrid

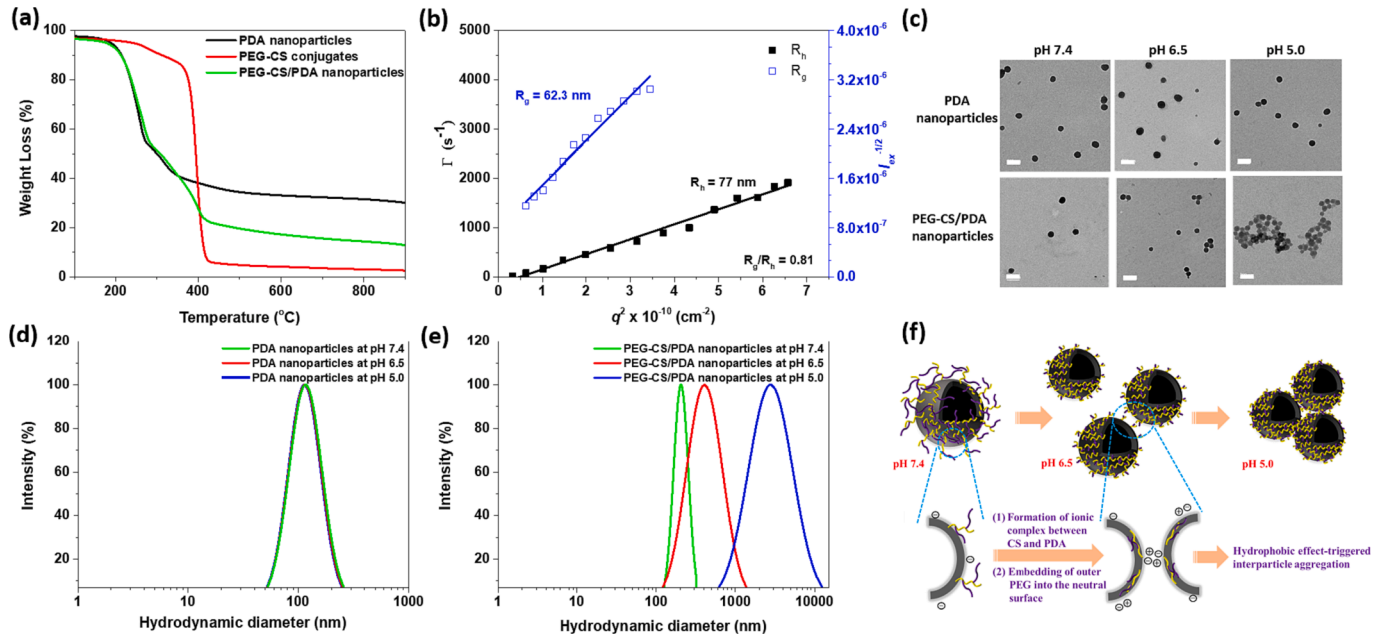

Fig. 3. (a) TGA profiles of PDA nanoparticles, PEG-CS conjugates and PEG-CS/PDA nanoparticles. (b) Berry plot for R_g and angle dependent correlation function of R_h of PEG-CS/PDA nanoparticles in pH 7.4 0.15 M PBS. (c) TEM images of pristine PDA nanoparticles and PEG-CS/PDA nanoparticles pretreated at pH 7.4, 6.5 and 5.0, respectively. Scale bars are 200 nm. DLS particle size distribution profiles of (d) PDA nanoparticles and (e) PEG-CS/PDA nanoparticles dispersed in aqueous solutions of different pH (ionic strength = 0.01 M). (f) Schematic illustration of acidity-triggered interparticle aggregation of PEG-CS/PDA nanoparticles.

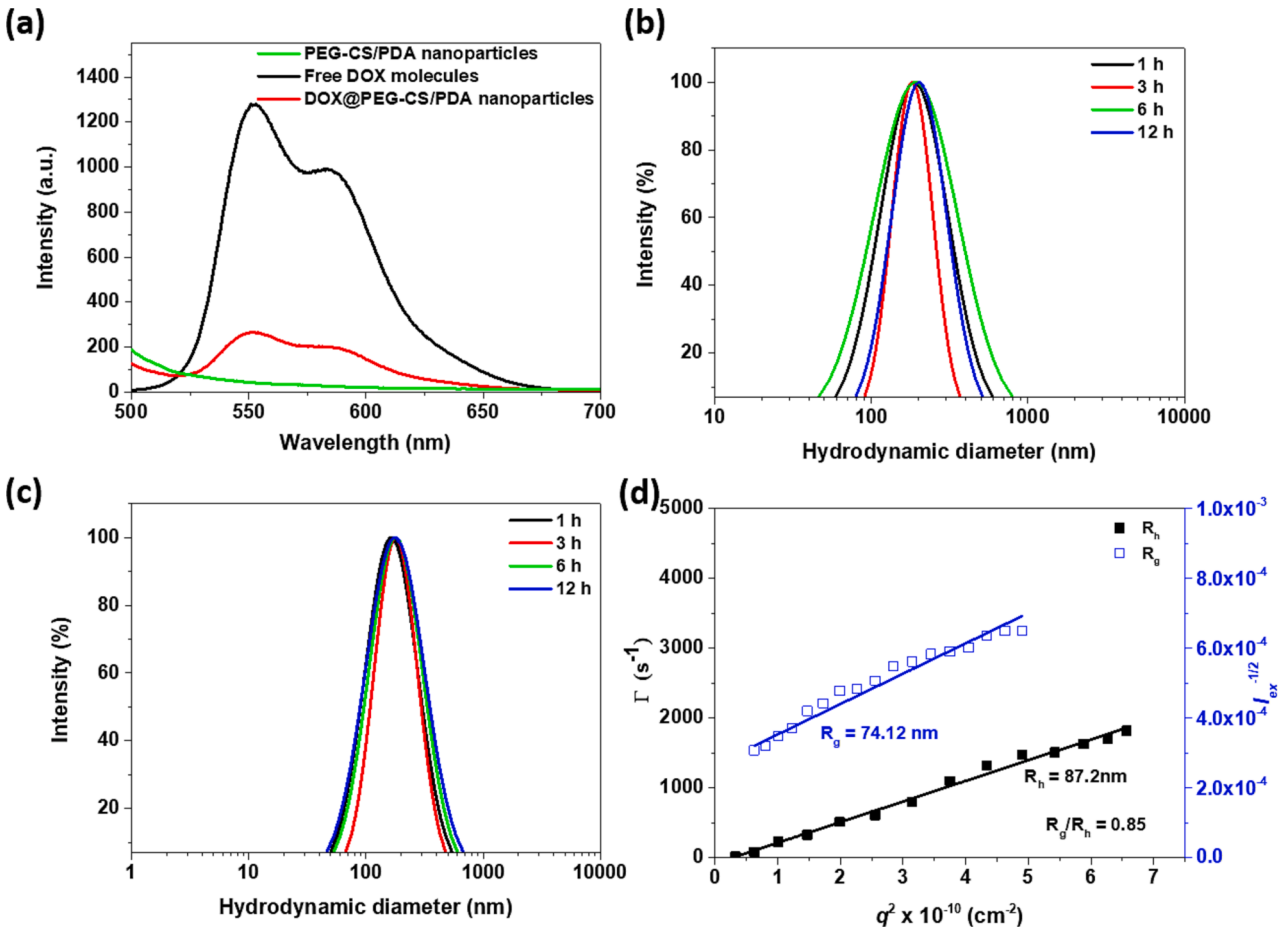

Fig. 4. (a) Fluorescence spectra of PEG-CS/PDA nanoparticles, free DOX molecules and DOX@PEG-CS/PDA nanoparticles in pH 7.4 PBS. DLS particle size distribution profiles of DOX@PEG-CS/PDA nanoparticles separately dispersed in (b) pH 7.4 0.15 M PBS and (c) 10 % FBS-containing PBS at different time intervals. (d) Berry plot for R_g and angle dependent correlation function of R_h of DOX@PEG-CS/PDA nanoparticles in pH 7.4 0.15 M PBS.

nanoparticles. As revealed in Table 1, compared to PEG-CS/PDA nanoparticles, the DOX@PEG-CS/PDA nanoparticles displayed somewhat larger particle size (ca 174.4 nm). It should be mentioned that the DOX@PEG-CS/PDA nanoparticles dispersed in pH 7.4 0.15 M PBS or 10 % FBS-containing PBS for 12 h still remained virtually unchanged particle size (Fig. 4b and c). This illustrates that the PEG-CS coating layer of DOX@PEG-CS/PDA nanoparticles could prevent inter-particle aggregation by inhibiting the non-specific adsorption of serum protein, thus promoting their colloidal stability. Besides, similar to PEG-CS/PDA nanoparticles, the DOX@PEG-CS/PDA nanoparticles exhibited nearly solid-like spherical shape in pH 7.4 0.15 M PBS as evidenced by angle-dependent DLS/SLS characterization (Fig. 4d).

Note that the DOX@PEG-CS/PDA nanoparticles undergoing the acidity-triggered protonation of chitosan segments and PEG shrinking tended to aggregate into large particles in response to pH reduction from 7.4 to 5.0 (Fig. 2e, 5a and 5b), being similar to drug-free PEG-CS/PDA nanoparticles. Considering the inherent weak acidity of the tumor microenvironment (pH_e 6.5 ~ 7.0), the acidity-activated inter-particle agglomeration of DOX@PEG-CS/PDA nanoparticles at pH 6.5 is expected to prolong their tumor retention time and reducing therapeutic nanoparticles removal by high interstitial pressure of tumor extracellular matrix. Similar concepts have been reported elsewhere [42,43]. Fig. 5c illustrates the pH-controlled drug release profiles of DOX@PEG-CS/PDA nanoparticles in aqueous solutions (ionic strength 0.15 M) at 37 °C. The cumulative drug release performed at pH 5.0 over a period of 6 h (ca 65.3 %) is appreciably higher than that (36.4 %) in pH 7.4 milieu. This is primarily attributed to that the hydrophobic and π - π stacking interaction between DOX molecules and PDA cores under acidic condition could be largely declined due to the increased protonation of DOX molecules. Such an accelerated DOX release from PDA-based nanoparticles in pH-dependent manner has been also observed in other studies [3,18,44,45]. Particularly, different from other DOX-carrying PDA nanoparticles that showed relatively low cumulative DOX release at pH 5.0 (below 20 % during 12 h) [31,44,45], the DOX@PEG-CS/PDA nanoparticles developed in this work largely promoted cumulative DOX liberation (over 70 %) under the same condition. Obviously, the acidity-elicited protonation of chitosan segments within PEG-CS layers could further facilitate liberation of positively-charged DOX molecules by repulsion force. Furthermore, it should be mentioned that the DOX@PEG-CS/PDA nanoparticles tended to aggregate at pH 5.0, thus probably resulting in the incomplete release of approximately 20% of the drug within 24 h.

For an ideal drug delivery system, in addition to controlled drug release, the effective biodegradation is highly required. In view of that the concentration of H_2O_2 in malignant tumor cells can be up to 100 μM, being much higher than that of normal cells (<20 nM) [46], H_2O_2 has emerged as a potential internal stimulus to promote degradation of nanovehicles. Notably, the DOX@PEG-CS/PDA nanoparticles in pH 7.4 0.15 PBS containing 0.4 mM H_2O_2 exhibited appreciably enlarged particle size over a period of 24 h, while the counterparts in PBS without H_2O_2 maintained nearly unchanged particle size over time (Fig. 5d). The SEM images in Fig. 5e also showed that the colloidal structure of DOX@PEG-CS/PDA nanoparticles after being pretreated with H_2O_2 was largely transformed from solid-like sphere to irregular and loose conformation. Similar results were also obtained for drug-free PEG-CS/PDA nanoparticles (Fig. 5d and e). Apparently, the DOX@PEG-CS/PDA nanoparticles could be effectively degraded in the presence of H_2O_2, being probably ascribed to decomposition of the PDA framework driven by oxidation of the phenolic hydroxyl groups [47]. Overall, the preliminary data suggest that PEG-CS/PDA nanoparticles hold promise for tumor-targeted drug delivery applications with excellent degradability.

3.4. Nir-triggered photothermal effect

Based on that the PDA nanoparticles are able to convert NIR into heat by non-radiative decay [48,49], the photothermal conversion effect of PEG-CS/PDA nanoparticles under irradiation of 808 nm NIR laser was explored to assess their feasibility in cancer photothermal therapy. As presented in Fig. 6a, under NIR irradiation, different from PBS with the nearly unchanged temperature, the aqueous solutions (pH 7.4 or 5.0) containing PDA nanoparticles or PEG-CS/PDA nanoparticles (PDA concentration = 100 μg/mL) showed remarkably raised temperature

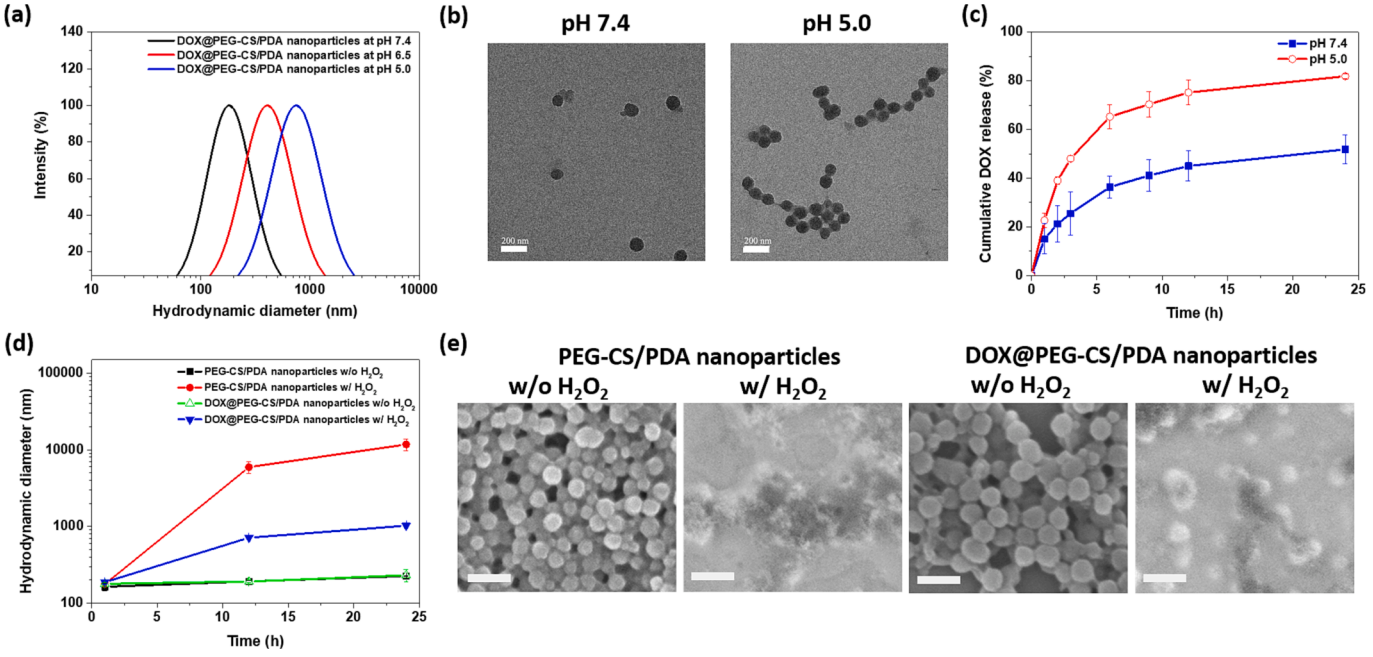

Fig. 5. (a) DLS particle size distribution profiles of DOX@PEG-CS/PDA nanoparticles in aqueous solution of different pH. (b) TEM images of DOX@PEG-CS/PDA nanoparticles pretreated at either pH 7.4 or 5.0. Scale bars are 200 nm. (c) Cumulative DOX release profiles of DOX@PEG-CS/PDA nanoparticles in aqueous solutions of pH 7.4 and 5.0 at 37 °C. (d) Hydrodynamic diameters of PEG-CS/PDA nanoparticles and DOX@PEG-CS/PDA nanoparticles dispersed in pH 7.4 0.15 M PBS containing H_2O_2 (0.4 mM) or not during 24 h. (e) SEM images of PEG-CS/PDA nanoparticles and DOX@PEG-CS/PDA nanoparticles with or without H_2O_2 pretreatment. Scale bars are 200 nm.

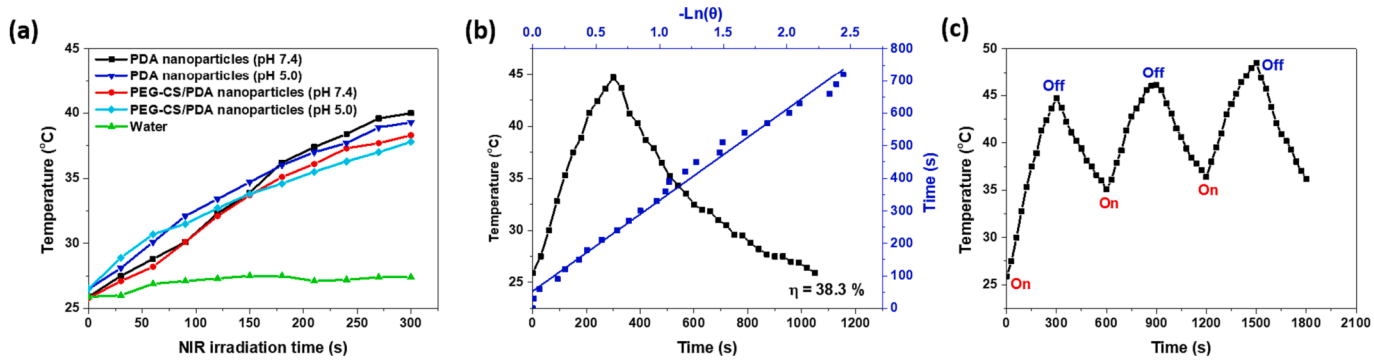

Fig. 6. (a) Temperature profiles of PDA and PEG-CS/PDA nanoparticles (PDA concentration: 100 μg/mL) in aqueous solutions (pH 7.4 or 5.0) with 808 nm NIR laser irradiation (1.0 W/cm^2). (b) Temperature profile of PEG-CS/PDA nanoparticle solution (PDA concentration: 200 μg/mL) exposed to 808 nm laser irradiation (1.0 W/cm^2) for single on/off cycle, and plot of cooling time versus negative logarithm of the temperature driving force. (c) Temperature changes of PEG-CS/PDA nanoparticle solution (PDA concentration: 200 μg/mL) during three on/off cycles of 808 nm laser irradiation (1.0 W/cm^2).

over 10 °C. Also, the NIR-triggered elevation of the temperature of PEG-CS/PDA nanoparticle solutions at pH 5.0 signifies that the acidity-induced interparticle aggregation could not impact their photothermal effect. Furthermore, the photothermal heating–cooling curve of PEG-CS/PDA nanoparticles was attainted (Fig. 6b) and their photothermal conversion efficiency was then calculated to be ca. 38.3 % similar to that of PDA nanoparticles (Fig. S7), indicating that the surface coating of PEG-CS adducts could not affect the photothermal conversion capability of PDA nanoparticles. It should be mentioned that the PEG-CS/PDA nanoparticles exhibited higher photothermal conversion efficiency than the previously reported photothermal agents such as copper sulfide nanoparticles (16.3 %) [50], gold nanorods (21.0 %) [51] and PDA nanoclustered micelles (22.2 %) [52]. Notably, with NIR laser irradiation of three on/off cycles, the maximum temperature of the aqueous solution containing PEG-CS/PDA nanoparticles showed no considerable change (Fig. 6c), demonstrating prominent photothermal stability of PEG-CS/PDA nanoparticles. As expected, the PEG-CS/PDA nanoparticles exhibited NIR-triggered photothermal capability in the laser power density- and concentration-dependent manner (Fig. S8). The above findings suggest that the PEG-CS/PDA nanoparticles show great potential of serving as photothermal agents for cancer photothermal therapy.

3.5. *In vitro cellular uptake and cytotoxicity*

The cellular internalization of DOX@PEG-CS/PDA nanoparticles by TRAMP-C1 cells was explored by CLSM. As presented in Fig. 7a, the DOX fluorescence intensity within TRAMP-C1 cells incubated with DOX@PEG-CS/PDA nanoparticles for 1 h was appreciably lower than that of cells treated with free DOX species. Such difference could be resulted from the different cellular uptake pathways for free DOX molecules (fast passive diffusion) and for DOX payloads delivered by nanoparticles (slow endocytosis) [53,54]. Moreover, with the incubation time being prolonged from 1 to 4 h, the accumulation of DOX transported by DOX@PEG-CS/PDA nanoparticles in the cytoplasm and nuclei of TRAMP-C1 cells was increased. Being consistent with the in vitro release results (Fig. 5c), DOX molecules were gradually liberated from DOX@PEG-CS/PDA nanoparticles entrapped within acidic endosome or lysosomes, thereby facilitating translocation of DOX into the nucleus regions.

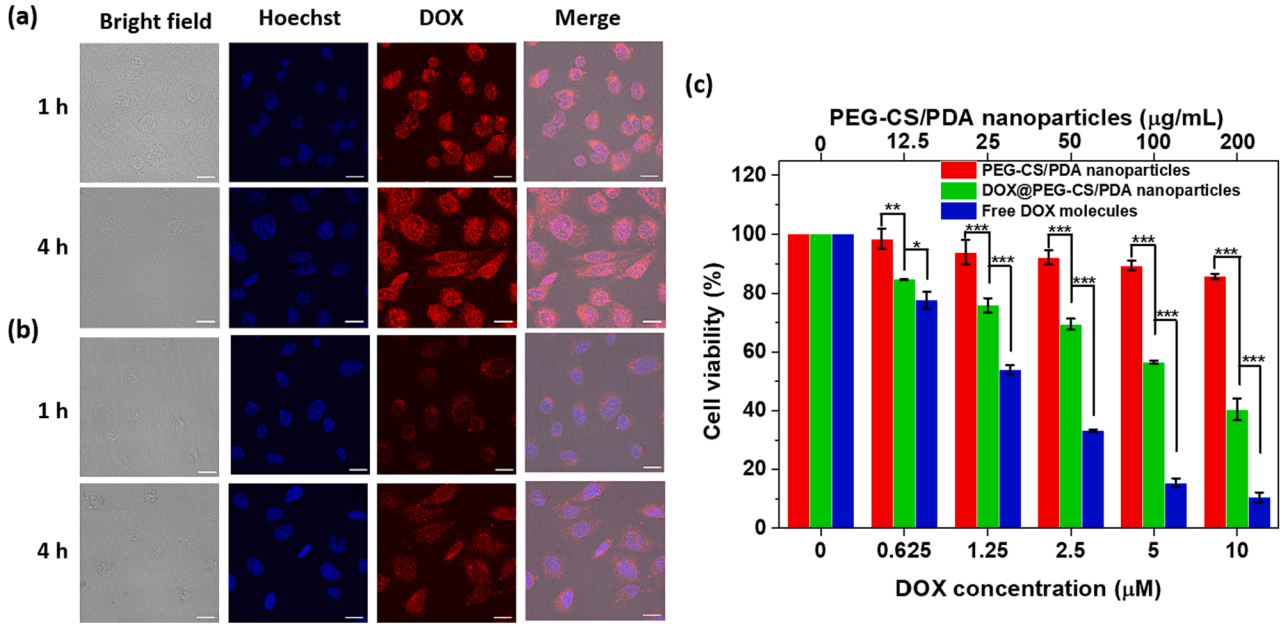

Fig. 7. CLSM images of TRAMP-C1 cells incubated with (a) free DOX molecules and (b) DOX@PEG-CS/PDA nanoparticles, respectively, for 1 and 4 h (DOX concentration = 10 μM). Scale bars are 20 μm. (c) Cell viability of TRAMP-C1 cells treated with PEG-CS/PDA nanoparticles, free DOX molecules and DOX@PEG-CS/PDA nanoparticles, respectively, at 37 °C for 24 h. *$p < 0.05$, **$p < 0.01$, ***$p < 0.001$.

The in vitro cytotoxicity of DOX@PEG-CS/PDA nanoparticles and free DOX molecules against TRAMP-C1 cells was determined by MTT assay as shown in Fig. 7b. As an important control, TRAMP-C1 cells incubated with drug-free PEG-CS/PDA nanoparticles in the concentration range 12.5 ~ 200 μg/mL for 24 h retained high viability (over 80 %), suggesting that the PEG-CS/PDA nanoparticles were nearly nontoxic to TRAMP-C1 cells. When TRAMP-C1 cells were incubated with free DOX molecules or DOX@PEG-CS/PDA nanoparticles in the drug concentration range 0.625 ~ 10 μM, the cell viability was significantly declined with increased drug concentration, being indicative of DOX-mediated cytotoxic effect via DNA double-strand breaks due to topoisomerase II inhibition. Notably, the attained drug doses required for 50 % cellular growth inhibition (IC_{50}) of free DOX molecules and DOX@PEG-CS/PDA nanoparticles are ca 1.35 and 7.33 μM, respectively, indicating that the DOX@PEG-CS/PDA nanoparticles exhibited somewhat lower anticancer activity compared to free DOX molecules. This could be attributed to that the time-consuming cellular internalization and drug release of DOX@PEG-CS/PDA nanoparticles resulted in the decrease of DOX-mediated cytotoxicity. Despite this, different from the non-specific tumor targeting of free DOX molecules, the DOX@PEG-CS/PDA nanoparticles were highly expected to be selectively deposited within tumor sites upon the EPR effect of solid tumors, thus promoting anticancer efficacy and reducing adverse effect.

4. Conclusions

To achieve effective intracellular DOX delivery, the photothermal PEG-CS/PDA nanoparticles as vehicles were successfully fabricated by the coating of PEG-CS conjugates on the surfaces of PDA nanoparticles upon Michael reaction. Based on the angle-dependent DLS/SLS data and TEM images, the PEG-CS/PDA nanoparticles were characterized to exhibit a well-dispersed spherical form in pH 7.4 aqueous solution. Due to the comprehensive π - π stacking and hydrophobic interactions of PDA and DOX, the DOX@PEG-CS/PDA nanoparticles exhibited satisfied drug loading capacity. Moreover, the DOX@PEG-CS/PDA nanoparticles not only maintained outstanding colloidal stability in FBS-containing 0.15 M PBS, but also rapidly degraded when exposed to H_2O_2-rich environment. In addition to remarkable inter-particle aggregation because of PEG embedding driven by formation of ionic CS/PDA complexes, the drug release of DOX@PEG-CS/PDA nanoparticles was appreciably accelerated in response to pH change from 7.4 to 5.0 by the enhanced repulsion force between protonated CS and DOX. The PEG-CS/PDA nanoparticles also showed robust photothermal effect and stability. After being internalized by TRAMP-C1 cells, the DOX@PEG-CS/PDA nanoparticles within acidic organelles progressively liberated DOX molecules, thereby promoting drug accumulation in nucleus to induce cell death. The results demonstrate the great potential of PEG-CS/PDA nanoparticles developed as DDS and photothermal agent for application of cancer treatment.

Declaration of Competing Interest

The authors declare that they have no known competing financial interests or personal relationships that could have appeared to influence the work reported in this paper.

Data availability

Data will be made available on request.

Acknowledgments

This work is supported by the National Science and Technology Council (MOST 110-2628-E-005-001, and MOST 111-2628-E-005-009-MY2), Taiwan.

Appendix A. Supplementary material

Supplementary data to this article can be found online at https://doi.org/10.1016/j.eurpolymj.2023.112365.

References

[1] K.e. Zheng, X. Liu, H. Liu, D. Dong, L. Li, L. Jiang, M. Huang, C. Ding, Novel pH-triggered doxorubicin-releasing nanoparticles self-assembled by functionalized β-cyclodextrin and amphiphilic phthalocyanine for anticancer therapy, ACS Appl. Mater. Interfaces 13 (9) (2021) 10674–10688.
[2] R.L. Siegel, K.D. Miller, A. Jemal, Cancer statistics, Ca-Cancer J. Clin. 69 (2019) 7–34.
[3] S.Y. Qin, A.Q. Zhang, X.Z. Zhang, Recent advances in targeted tumor chemotherapy based on smart nanomedicines, Small 14 (2018) 1802417.
[4] K.S. Crider, T.P. Yang, R.J. Berry, L.B. Bailey, Folate and DNA methylation: a review of molecular mechanisms and the evidence for folate's role, Adv. Nutr. 3 (2012) 21–38.
[5] P. Liu, G. Chen, J. Zhang, A Review of liposomes as a drug delivery system: current status of approved products, regulatory environments, and future perspectives, Molecules 27 (2022) 1372.
[6] D. Guimarães, A. Cavaco-Paulo, E. Nogueira, Design of liposomes as drug delivery system for therapeutic applications, Int. J. Pharm. 601 (2021), 120571.
[7] S.Y. Huang, N.T. Yeh, T.H. Wang, T.C. Hsu, H.Y. Chin, B.S. Tzang, W.H. Chiang, Onion-like doxorubicin-carrying polymeric nanomicelles with tumor acidity-sensitive dePEGylation to expose positively-charged chitosan shell for enhanced cancer chemotherapy, Int. J. Biol. Macromol. 227 (2023) 925–937.
[8] X. Zhang, T. Zhu, Y. Miao, L. Zhou, W. Zhang, Dual-responsive doxorubicin-loaded nanomicelles for enhanced cancer therapy, J. Nanobiotechnol. 18 (2020) 136.
[9] R. Mrowczyń ski,, Polydopamine-based multifunctional (Nano)materials for cancer therapy, ACS Appl, Mater. Interfaces 10 (2018) 7541–7561.
[10] Y. Song, C.-M. Dong, Sugar-dependent targeting and immune adjuvant effects of hyperbranched glycosylated polypeptide nanoparticles for ovalbumin delivery, Chin. Chem. Lett. 33 (8) (2022) 4084–4088.
[11] S.C. Thomas, P.K. Harshita, S. Mishra, Talegaonkar, Ceramic nanoparticles: fabrication methods and applications in drug delivery, Curr. Pharm. Des. 21 (2015) 6165–6188.
[12] Z. Li, Y. Yang, H. Wei, X. Shan, X. Wang, M. Ou, Q. Liu, N. Gao, H. Chen, L. Mei, X. Zeng, Charge-reversal biodegradable MSNs for tumor synergetic chemo/photothermal and visualized therapy, J. Control. Release 338 (2021) 719–730.
[13] Z. Li, Y. Yu, W. Zeng, F. Ding, D. Zhang, W. Cheng, M. Wang, H. Chen, G. Pan, L. Mei, X. Zeng, N. Gao, Mussel-inspired ligand clicking and ion coordination on 2D black phosphorus for cancer multimodal imaging and therapy, Small 18 (2022) 2201803.
[14] P. Horcajada, T. Chalati, C. Serre, B. Gillet, C. Sebrie, T. Baati, J.F. Eubank, D. Heurtaux, P. Clayette, C. Kreuz, J.S. Chang, Y.K. Hwang, V. Marsaud, P. N. Bories, L. Cynober, S. Gil, G. Férey, P. Couvreur, R. Gref, Porous metal-organic-framework nanoscale carriers as a potential platform for drug delivery and imaging, Nat. Mater. 9 (2010) 172–178.
[15] S. He, L.i. Wu, X. Li, H. Sun, T. Xiong, J. Liu, C. Huang, H. Xu, H. Sun, W. Chen, R. Gref, J. Zhang, Metal-organic frameworks for advanced drug delivery, Acta Pharm. Sin. B 11 (8) (2021) 2362–2395.
[16] H. Wu, H. Hu, J. Wan, Y. Li, Y. Wu, Y. Tang, C. Xiao, H. Xu, X. Yang, Z. Li, Hydroxyethyl starch stabilized polydopamine nanoparticles for cancer chemotherapy, Chem. Eng. J. 349 (2018) 129–145.
[17] H. Wu, M. Wei, Y. Xu, Y. Li, X. Zhai, P. Su, Q. Ma, H. Zhang, PDA-based drug delivery nanosystems: a potential approach for glioma treatment, Int. J. Nanomed. 17 (2022) 3751–3775.
[18] M.H. Hsieh, T.H. Wang, S.H. Hu, T.C. Hsu, J.L. Yow, B.S. Tzang, W.H. Chiang, Tumor site-specific PEG detachment and active tumor homing of therapeutic PEGylated chitosan/folate-decorated polydopamine nanoparticles to augment antitumor efficacy of photothermal/chemo combination therapy, Chem. Eng. J. 446 (2022), 137243.
[19] Z. Li, Z. Chen, H. Chen, K. Chen, W. Tao, X.K. Ouyang, L. Mei, X. Zeng, Polyphenol-based hydrogels: Pyramid evolution from crosslinked structures to biomedical applications and the reverse design, Bioact. Mater. 17 (2022) 49–70.
[20] P. Huang, Y. Yang, W. Wang, Z. Li, N. Gao, H. Chen, X. Zeng, Self-driven nanoprodrug platform with enhanced ferroptosis for synergistic photothermal-IDO immunotherapy, Biomaterials 299 (2023), 122157.
[21] Y. Yang, W. Zeng, P. Huang, X. Zeng, L. Mei, Smart materials for drug delivery and cancer therapy, VIEW 2 (2021) 20200042.
[22] C. Du, X. Wu, M. He, Y. Zhang, R. Zhang, C.M. Dong, Polymeric photothermal agents for cancer therapy: recent progress and clinical potential, J. Mater. Chem. B 9 (2021) 1478-1490.
[23] B. Poinard, S.Z.Y. Neo, E.L.L. Yeo, H.P.S. Heng, K.G. Neoh, J.C.Y. Kah, Polydopamine nanoparticles enhance drug release for combined photodynamic and photothermal therapy, ACS Appl. Mater. Interfaces 10 (25) (2018) 21125–21136.
[24] L.-P. Zhu, J.-H. Jiang, B.-K. Zhu, Y.-Y. Xu, Immobilization of bovine serum albumin onto porous polyethylene membranes using strongly attached polydopamine as a spacer, Colloids Surf. B Biointerfaces 86 (1) (2011) 111–118.
[25] S. Liu, J. Pan, J. Liu, Y. Ma, F. Qiu, L. Mei, X. Zeng, G. Pan, Dynamically PEGylated and borate-coordination-polymer-coated polydopamine nanoparticles for

synergetic tumor-targeted, chemo-photothermal combination therapy, Small 14 (2018) 1703968.
[26] J. Hong, Y. Tang, M. Zhou, J. Deng, H. Hu, D. Xu, Polyethylene glycol-modified mesoporous polydopamine nanoparticles co-loaded with dimethylcurcumin and indocyanine green for combination therapy of castration-resistant prostate cancer, J. Drug Deliv. Sci. Technol. 69 (2022), 103158.
[27] X. Yu, X. Tang, J. He, X. Yi, G. Xu, L. Tian, R. Zhou, C. Zhang, K. Yang, Polydopamine nanoparticle as a multifunctional nanocarrier for combined radiophotodynamic therapy of cancer, Part. Part. Syst. Char. 34 (2017) 1600296.
[28] C. Chen, W. Tang, D. Jiang, G. Yang, X. Wang, L. Zhou, W. Zhang, P. Wang, Hyaluronic acid conjugated polydopamine functionalized mesoporous silica nanoparticles for synergistic targeted chemo-photothermal therapy, Nanoscale 11 (22) (2019) 11012–11024.
[29] Y. Yu, S.-J. Zhu, H.-T. Dong, X.-Q. Zhang, J.-A. Li, S.-K. Guan, A novel MgF2/PDA/S-HA coating on the bio-degradable ZE21B alloy for better multi-functions on cardiovascular application, J. Magnes. Alloy 11 (2) (2023) 480–492.
[30] X. Li, H. Lu, Y. Zhang, F. He, L. Jing, X. He, Fabrication of magnetic alginate beads with uniform dispersion of CoFe2O4 by the polydopamine surface functionalization for organic pollutants removal, Appl. Surf. Sci. 389 (2016) 567–577.
[31] L. Wang, W. Dai, M. Yang, X. Wei, K. Ma, B. Song, P. Jia, Y. Gong, J. Yang, J. Zhao, Cell membrane mimetic copolymer coated polydopamine nanoparticles for combined pH-sensitive drug release and near-infrared photothermal therapeutic, Colloids Surf. B Biointerfaces 176 (2019) 1–8.
[32] S. Chen, L. Li, C. Zhao, J. Zheng, Surface hydration: Principles and applications toward low-fouling/nonfouling biomaterials, Polymer 51 (2010) 5283–5293.
[33] J.M. Harris, R.B. Chess, Effect of pegylation on pharmaceuticals, Nat. Rev. Drug Discov. 2 (3) (2003) 214–221.
[34] F.M. Veronese, G. Pasut, PEGylation, successful approach to drug delivery, Drug Discov. Today 10 (21) (2005) 1451–1458.
[35] X. Zhong, K. Yang, Z. Dong, X. Yi, Y. Wang, C. Ge, Y. Zhao, Z. Liu, Polydopamine as a biocompatible multifunctional nanocarrier for combined radioisotope therapy and chemotherapy of cancer, Adv. Funct. Mater. 25 (47) (2015) 7327–7336.
[36] S.J. Huang, T.H. Wang, Y.H. Chou, H.M.D. Wang, T.C. Hsu, J.L. Yow, B.S. Tzang, W.H. Chiang, Hybrid PEGylated chitosan/PLGA nanoparticles designed as pH-responsive vehicles to promote intracellular drug delivery and cancer chemotherapy, Int. J. Biol. Macromol. 210 (2022) 565–578.
[37] A.E. Smith, X. Xu, S.E. Kirkland-York, D.A. Savin, C.L. McCormick, Schizophrenic self-assembly of block copolymers synthesized via aqueous RAFT polymerization: From micelles to vesicles, Macromolecules 43 (2010) 1210–1217.
[38] Y.-H. Chou, Y.-L. Liu, T.-C. Hsu, J.-L. Yow, B.-S. Tzang, W.-H. Chiang, Tumor acidity-responsive polymeric nanoparticles to promote intracellular delivery of zoledronic acid by PEG detachment and positive charge exposure for enhanced antitumor potency, J. Mater. Chem. B 10 (23) (2022) 4363–4374.
[39] K. Kogej, D. Božič, B. Kobal, M. Herzog, K. Černe, Application of dynamic and static light scattering for size and shape characterization of small extracellular nanoparticles in plasma and ascites of ovarian cancer patients, Int. J. Mol. Sci. 22 (2021) 12946.
[40] C. Wu, S. Zhou, Laser light scattering study of the phase transition of poly(N-isopropylacrylamide) in water. 1. Single chain, Macromolecules 28 (24) (1995) 8381–8387.
[41] W. Qiang, W. Li, X. Li, X. Chen, D. Xu, Bioinspired polydopamine nanospheres: a superquencher for fluorescence sensing of biomolecules, Chem. Sci. 5 (8) (2014) 3018–3024.
[42] H. Li, Y. Chen, Z. Li, X.u. Li, Q. Jin, J. Ji, Hemoglobin as a smart pH-sensitive nanocarrier to achieve aggregation enhanced tumor retention, Biomacromolecules 19 (6) (2018) 2007–2013.
[43] X. Cheng, X. Zhou, J. Xu, R. Sun, H. Xia, J. Ding, Y.E. Chin, Z. Chai, H. Shi, M. Gao, Furin enzyme and pH synergistically triggered aggregation of gold nanoparticles for activated photoacoustic imaging and photothermal therapy of tumors, Anal. Chem. 93 (26) (2021) 9277–9285.
[44] Y. Xing, J. Zhang, F. Chen, J. Liu, K. Cai, Mesoporous polydopamine nanoparticles with co-delivery function for overcoming multidrug resistance via synergistic chemo-photothermal therapy, Nanoscale 9 (25) (2017) 8781–8790.
[45] D. Ren, G.R. Williams, Y. Zhang, R. Ren, J. Lou, L.-M. Zhu, Mesoporous doxorubicin-loaded polydopamine nanoparticles coated with a platelet membrane suppress tumor growth in a murine model of human breast cancer, ACS Appl. Bio Mater. 5 (1) (2022) 123–133.
[46] Y. Wu, T. Guo, Y. Qiu, Y. Lin, Y. Yao, W. Lian, L. Lin, J. Song, H. Yang, An inorganic prodrug, tellurium nanowires with enhanced ROS generation and GSH depletion for selective cancer therapy, Chem. Sci. 10 (29) (2019) 7068–7075.
[47] J.-H. Lin, C.-J. Yu, Y.-C. Yang, W.-L. Tseng, Formation of fluorescent polydopamine dots from hydroxyl radical-induced degradation of polydopamine nanoparticles, PCCP 17 (23) (2015) 15124–15130.
[48] W. Cheng, X. Zeng, H. Chen, Z. Li, W. Zeng, L. Mei, Y. Zhao, Versatile polydopamine platforms: Synthesis and promising applications for surface modification and advanced nanomedicine, ACS Nano 13 (2019) 8537–8565.
[49] Y. Zou, X. Chen, P. Yang, G. Liang, Y. Yang, Z. Gu, Y. Li, Regulating the absorption spectrum of polydopamine, Sci. Adv. 6 (2020) eabb4696.
[50] S. Wang, A. Riedinger, H. Li, C. Fu, H. Liu, L. Li, T. Liu, L. Tan, M.J. Barthel, G. Pugliese, F. De Donato, M.S. D'Abbusco, X. Meng, L. Manna, H. Meng, T. Pellegrino, Plasmonic copper sulfide nanocrystals exhibiting near-infrared photothermal and photodynamic therapeutic effects, ACS Nano 9 (2015) 1788.
[51] C.M. Hessel, V.P. Pattani, M. Rasch, M.G. Panthani, B. Koo, J.W. Tunnell, B. A. Korgel, Copper selenide nanocrystals for photothermal therapy, Nano Lett. 11 (6) (2011) 2560–2566.
[52] Y. Xing, T. Ding, Z. Wang, L. Wang, H. Guan, J. Tang, D. Mo, J. Zhang, Temporally controlled photothermal/photodynamic and combined therapy for overcoming multidrug resistance of cancer by polydopamine nanoclustered micelles, ACS Appl. Mater. Interfaces 11 (15) (2019) 13945–13953.
[53] X.T. Shuai, H. Ai, N. Nasongkla, S.J. Kim, J.M. Gao, Micellar carriers based on block copolymers of poly(epsilon-caprolactone) and poly(ethylene glycol) for doxorubicin delivery, J. Control. Release 98 (2004) 415–426.
[54] P. Liang, D. Zhao, C.Q. Wang, J.Y. Zong, R.X. Zhuo, S.X. Cheng, Facile preparation of heparin/CaCO3/CaP hybrid nano-carriers with controllable size for anticancer drug delivery, Colloids Surf. B 102 (2013) 783–788.